ACS OMEGA

http://pubs.acs.org/journal/acsodf

Article

Unveiling the Role of Precursors in the Byproduct Formation of AgCl-Replicated Bimetallic Nanostructures and Their Stability-Dependent Photothermal Properties

Han-Jung Ryu, Kyung Tae Kim, Won Kyu Lee, and Jae-Seung Lee*

Cite This: *ACS Omega* 2023, 8, 25506−25514

Read Online

ACCESS | Metrics & More | Article Recommendations | Supporting Information

ABSTRACT: AgCl nanomaterials recently attracted scientific interest as useful structural building blocks for producing metallic nanomaterials owing to their facile synthesis, controllable morphology, and ease of removal under ambient conditions. However, their complex chemical reactivity has primarily been studied in association with water solubility or reducibility. This study investigates the pivotal role of precursor ligands in the photochemical synthesis of metallic cubic mesh nanostructures on the AgCl templates. The side reactions between AgCl and Au precursors with different ligands are thoroughly discussed along with their influence on the byproduct formation and the structural stability of the resulting metallic nanostructures. Importantly, we introduce for the first time the partial destruction of AgCl and the formation of undesirable byproducts caused by the presence of highly oxidizing and Cl-containing $AuCl_4^-$. In addition, a synthetic route for producing highly pure and stable metallic nanostructures using a halogen-free Au precursor or Pt-priming is proposed. Further, the photothermal properties of these replicated metallic nanostructures are presented as a new evaluation tool for analyzing their overall structural stability. Discovering the role of precursor ligands in the reaction system will prove useful as a guide for the synthesis of functional noble metal nanomaterials using silver halide templates.

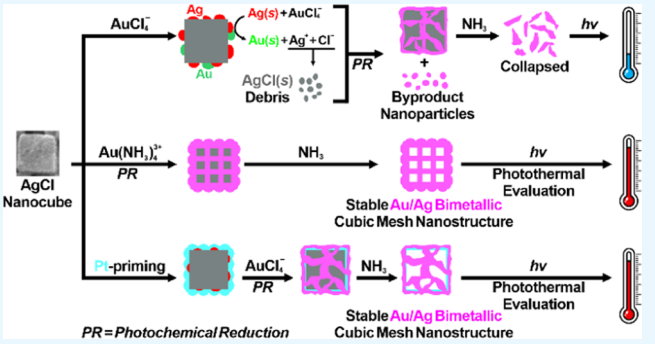

INTRODUCTION

Recently, AgCl nanoparticles (AgCl NPs) have received increased interest as efficient structural building blocks for the synthesis of nanomaterials with controlled shapes and sizes.[1−8] Many multimetallic nanomaterials are currently synthesized by constructing three-dimensional cubic and spherical mesh nanostructures using AgCl NPs as templates due to the excellent chemical and physical properties of AgCl, such as rapid and facile synthesis at room temperature, controllable shapes and sizes, and cost-effectiveness.[9,10] Easy removal of the AgCl template with a dilute NH_3 solution is a significant advantage in a sacrificial template compared to other inorganic and organic nano-templates. Moreover, AgCl itself can play a role as a reactive Ag precursor under precise chemical control, which significantly increases interfacial fabrication between the template and metallic replica. However, the high reactivity of AgCl can be a double-edged sword. For example, the undesired reduction of AgCl in the presence of reductants or under light irradiation may result in the self-nucleation and growth of byproduct Ag NPs, which deteriorate the homogeneity of the final products.[11,12] Moreover, the dissolution of AgCl can be easily induced by inorganic ligands other than NH_3.[13] Therefore, there is a need to develop a precise chemical control of the metallic replication without the deformation of AgCl templates.

Ligand is one of the most powerful tools to control the reduction chemistry of metallic precursors as their chemical properties, such as standard reduction potentials, solubility, and stability, are governed by coordinated ligands. Reduction pathways and resultant nanostructures are often controlled by ligand exchange.[14,15] For gold precursors, tetrachloroauric acid ($HAuCl_4$) is widely considered as the exclusive precursor for the synthesis of Au-based nanostructures, as demonstrated as early as the 1950s.[16] Based on its high standard reduction potential and good solubility in various solvents, $HAuCl_4$ is conventionally favored with incorporation into various synthetic methods. However, $HAuCl_4$ may be problematic during the synthesis as its high reducibility offers potential as a strong oxidizing agent, which may result in the oxidative destruction of preceding metallic nanostructures during the

Received: May 5, 2023
Accepted: June 20, 2023
Published: July 7, 2023

synthesis through a galvanic replacement reaction. Additionally, the Cl^- ligands are released in the aqueous reaction media through ligand exchange with hydroxide ions, which is uncontrollable during the synthesis.[17] The released Cl^- ions can form undesirable byproducts that significantly degrade the purity of resultant nanomaterials and disturb the application of synthesized nanomaterials by blocking their surfaces.[18] Cl^- ions also reverse the electrostatic charge of Au^{3+} ions from positive to negative, thereby limiting the electrostatic interaction-based utilization of Au^{3+} ions. As an alternative, the halogen-free positive Au precursor, $Au(NH_3)_4(NO_3)_3$, was recently adopted for the synthesis of Au-DNA nanoparticles based on their electrostatic interactions.[19] The usage of the halogen-free precursor may improve the structures and expand applications of Au-based nanostructures by suppressing side reactions and the formation of byproducts. Therefore, the choice of suitable Au precursors is essential for expanding the usage of Au-based nanomaterials with desired functions.

In this study, the photochemical replication of metallic cubic mesh nanostructures (CMNs) on AgCl templates (AgCl@CMN) using two types of Au precursors ($HAuCl_4$ and $Au(NH_3)_4(NO_3)_3$) is demonstrated. To date, such CMNs have demonstrated themselves as efficient photocatalysts and SERS probes.[2,5,6] Further, this study also reports that the use of the halogen-free Au precursor fundamentally prevents the chemical formation of undesired and unremovable AgCl debris and consequent byproduct NPs caused by using $HAuCl_4$ precursor. To protect the AgCl surface, another bypass method, Pt-priming, is also proposed to effectively prevent undesired reactions with $HAuCl_4$. Additionally, the photothermal properties of the CMNs are demonstrated as a useful measure for evaluating the structural stability of the replicated nanostructures.

EXPERIMENTAL SECTION

Materials and Instruments. Silver nitrate (cat. No. 204390), gold(III) chloride trihydrate (cat. No. 520918), potassium tetrachloroplatinate(II) (cat. No. 323411), sodium citrate tribasic dihydrate (cat. No. S4641), polyvinylpyrrolidone (PVP, cat. No. 856568; M_w 10 000), L-ascorbic acid (cat. No. A5960), ammonium hydroxide solution (cat. No. 221228), and Tween 20 (cat. No. P9416) were purchased from Sigma-Aldrich (St. Louis, Missouri). Tetramine gold nitrate ($Au(NH_3)_4(NO_3)_3$) was synthesized according to a published method.[20] Ultrapure water obtained from a Millipore Direct-Q3 system (18.2 MΩ·cm; Millipore, Billerica, Massachusetts) was used for all experiments. A metal halide lamp was purchased from Koryo Industry (400 W; Seoul, Republic of Korea). An 808 nm laser was purchased from Changchun New Industries Optoelectronics Tech. Co., Ltd. (MDL-III-808 nm-1W; Changchun, China). The structural, surface, and optical properties were observed using scanning electron microscopy (SEM; Quanta 250 FEG, FEI), transmission electron microscopy (TEM; Talos F200X (FEI) operated at 200 kV, and Titan Themis 3 (FEI) operated at 300 kV), X-ray photoelectron spectroscopy (XPS; K-Alpha X-ray Photoelectron Spectrometer System, Thermo Fisher Scientific, Waltham, Massachusetts), UV−vis spectroscopy (UV−vis; Agilent 8453, Agilent Technologies, Santa Clara, California), dynamic light scattering (DLS) and zeta potential measurement (Zetasizer Nano ZS90, Malvern Panalytical, Malvern, UK), and inductively coupled plasma mass spectrometry (ICP-MS; Agilent 7700, Agilent Technologies, Santa Clara, California).

Synthesis of AgCl Nanocubes (NCs) and AgCl Nanospheres (NSs). An aqueous $HAuCl_4$ solution (5 mM, 100 μL) and PVP (5.59 g/L, 15 μL) were added to 7.5 mL of ultrapure water. An $AgNO_3$ solution (5 mM, 190 μL) was introduced into the mixture (7.805 mL in total; final [$HAuCl_4$], [PVP], and [$AgNO_3$] = 64 μM, 0.0107 g/L, and 0.122 mM, respectively) after 5 min, followed by incubation of the solution for 30 min at 25 °C under dark conditions with vigorous stirring. The resultant mixture solution appeared white opaque owing to the presence of synthesized AgCl NCs and was centrifuged at a speed of 5000 rpm (2348 rcf) for 5 min. The supernatant was removed, and the AgCl NCs were redispersed in a 0.01% Tween 20 solution. Assuming complete conversion of the given number of Ag^+ ions (9.5×10^{-7} mol), the calculated mole number of the AgCl NCs was 5.08 fmol (edge length and density of the AgCl NCs are 200 nm and 5.56 g/cm^3, respectively). The AgCl NSs were synthesized following the same procedure, except for a higher final PVP concentration (1.611 g/L).

Photochemical Synthesis of Metallic Cubic Mesh Nanostructures (CMNs) and Spherical Mesh Nanostructures (SMNs) without Pt-Priming. The AgCl NCs (5.08 fmol) were dispersed in 6.79 mL of ultrapure water and combined with aqueous PVP (5.59 g/L, 15 μL), trisodium citrate (5 mM, 500 μL), and one of the Au precursors ($HAuCl_4$ or $Au(NH_3)_4(NO_3)_3$; 1 mM, 500 μL). A 400 W metal halide lamp was placed 25 cm away from the reaction vessel, which underwent light irradiation for 30 min along with vigorous stirring at 25 °C. The resultant nanomaterials solution was centrifuged at a speed of 5000 rpm (2348 rcf) for 5 min. The supernatant was removed and the AgCl@CMNs were redispersed in a 0.01% Tween 20 solution. The SMNs were synthesized using the AgCl NSs instead of the AgCl NCs. To remove the AgCl core, the AgCl@CMNs (or AgCl@SMNs) were incubated in a 3 wt % NH_3 solution for 30 min and vigorously stirred. For further purification, the products were centrifuged at a speed of 5000 rpm (2348 rcf) for 5 min, the supernatant was removed, and the products were redispersed in a 0.01% Tween 20 solution.

Photochemical Synthesis of Metallic CMNs and SMNs with Pt-Priming. The photochemical synthesis of the Pt-primed CMNs was performed with the two-step photochemical reduction. For the Pt-priming on the AgCl NCs, the synthesized AgCl NCs (5.08 fmol) were dispersed in 7.19 mL of ultrapure water, followed by the addition of PVP (5.59 g/L, 15 μL), trisodium citrate (5 mM, 500 μL), and K_2PtCl_4 (5 mM, 100 μL). The photochemical reduction and purification were conducted as described above. For the synthesis of the AgCl@CMNs, the Pt-primed AgCl NCs were dispersed in 7.04 mL of ultrapure water, followed by the addition of PVP (5.59 g/L, 15 μL), trisodium citrate (5 mM, 250 μL), and $HAuCl_4$ (1 mM, 500 μL). The photochemical reduction and purification were repeated to produce AgCl@CMNs. The SMNs were synthesized using the Pt-primed AgCl NSs instead of Pt-primed AgCl NCs. The removal of AgCl and the product purification were conducted as described above.

Measurement of Photothermal Properties. To monitor the photothermal properties, the AgCl@CMNs and CMNs (each synthesized from 10.16 fmol of AgCl NCs) were dispersed in 2 mL of ultrapure water. The resultant mixture was vigorously stirred to prevent sedimentation, and

https://doi.org/10.1021/acsomega.3c03096
ACS Omega 2023, 8, 25506−25514

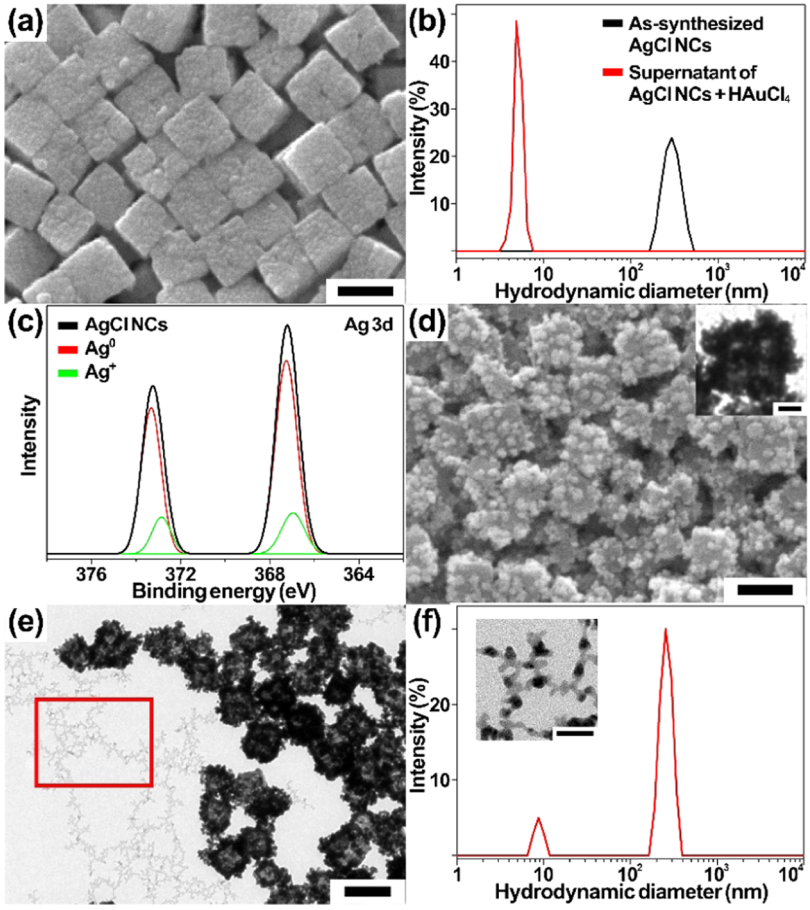

Figure 1. (a) SEM image of AgCl NCs after reaction with $HAuCl_4$ under dark conditions. (b) Size distributions of as-synthesized AgCl NCs and the isolated supernatants after the addition of $HAuCl_4$. The tiny debris was observed separately due to their significantly weak scattering. (c) XPS fine scan of Ag 3d of as-synthesized AgCl NCs. (d) SEM image of AgCl@CMNs synthesized by photochemical reduction of $HAuCl_4$ on AgCl NCs. (Inset) Single AgCl@CMN observed using TEM. The scale bar of the inset is 30 nm. (e) TEM image of AgCl@CMNs observed in a large area, showing a significant number of byproduct NPs. (f) Size distribution of the AgCl@CMNs. (Inset) Magnified TEM image of the byproduct NPs in the red box of Figure 1e. All of the scale bars are 200 nm except that of the inset which is 30 nm.

the temperature was measured under irradiation of near-infrared light using an 808 nm laser at 1 W/cm^2.

RESULTS AND DISCUSSION

The chemistry of AgCl is complicated; it is associated with the coordination and redox reactions of Ag^+, both of which are affected by the type of precursor ligands and reductants. Owing to AgCl's high reducibility (E° = 0.222 V), it can be deformed during the reduction reaction, resulting in a failed replication for the synthesis of metallic nanostructures. In fact, when we attempted to reduce Au^{3+} on AgCl NC templates using ascorbic acid for the metallic replication, they significantly destructed into smaller particles, which occurred regardless of the types of Au^{3+} precursors (see the Supporting Information, Figure S1). To mitigate this issue, a photochemical synthetic route was designed with light-intensity-dependent milder reductive conditions that favor the preservation of the AgCl NCs and the reduction of Au precursors. Before light irradiation, the as-synthesized AgCl NCs were combined with $HAuCl_4$ and examined using SEM (Figure 1a). As expected, the AgCl NCs exhibited negligible structural changes after the mixing, as both Ag^+ and Au^{3+} ions are in their highest oxidation states and will not react with each other. Surprisingly, the DLS analysis of the AgCl NCs combined with $AuCl_4^-$ revealed the presence of a certain proportion of tiny debris (~5 nm in diameter), which was not observed with the as-synthesized AgCl NCs (Figure 1b). The supernatant from the mixture of AgCl NCs and $HAuCl_4$ containing debris was elementally analyzed using ICP-MS, and it was compared with the supernatant from a pure AgCl NC solution. Interestingly, the debris solution contained 17 times as many Ag^+ ions as the supernatant from the pure AgCl NC solution. The hypothesis is that the debris was composed of AgCl, which was formed from Cl^- released from $AuCl_4^-$ and Ag^+ obtained from the oxidation of Ag^0 on the AgCl NCs by $AuCl_4^-$ (E° of $AuCl_4^-$ = 1.005 V and E° of Ag^+ = 0.800 V) via the following chemical reactions (stoichiometric coefficients are omitted for simplicity).[21]

$$AgCl(s) + h\nu \rightarrow Ag^0(s) + Cl_2(g) \quad (1)$$

$$Ag^0(s) + AuCl_4^-(aq) \rightarrow Ag^+(aq) + Cl^-(aq) + Au^0(s) \quad (2)$$

$$Ag^+(aq) + Cl^-(aq) \rightarrow AgCl(s)\downarrow \quad (3)$$

To investigate this hypothesis, XPS was used to examine the presence of Ag^0 on the AgCl NCs, which is widely known to be formed due to the reduction of photosensitive AgCl to Ag (Figure 1c).[22,23] Despite the synthesis under dark conditions, Ag^0 coexisting with Ag^+ on the AgCl NCs was observed as

https://doi.org/10.1021/acsomega.3c03096
ACS Omega 2023, 8, 25506−25514

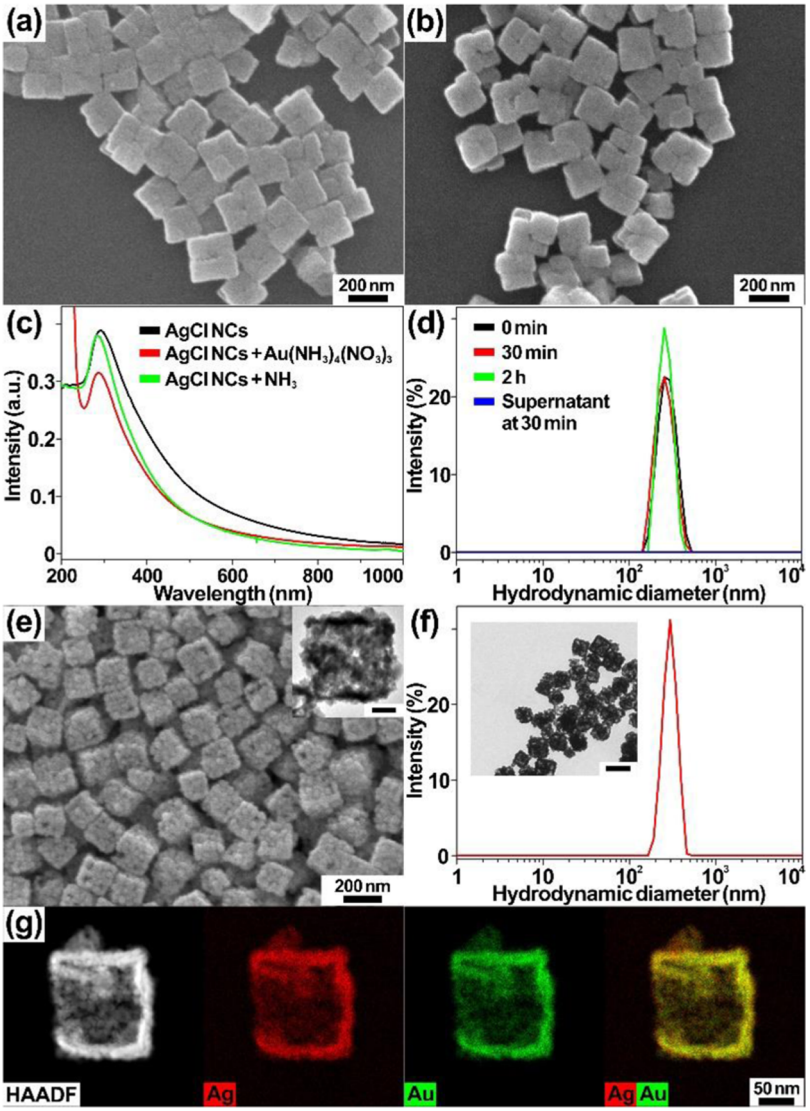

Figure 2. SEM images of AgCl NCs after reaction with (a) $Au(NH_3)_4(NO_3)_3$ and (b) NH_3. The concentration of NH_3 in (b) was four times higher than that of $Au(NH_3)_4^{3+}$ in (a). (c) UV−vis spectra of as-synthesized AgCl NCs and the resultant mixture after reaction with $Au(NH_3)_4(NO_3)_3$ and NH_3. (d) Time-dependent size distributions of AgCl NCs after their reaction with $Au(NH_3)_4(NO_3)_3$. (e) SEM image of AgCl@CMNs synthesized by photochemical reduction. (Inset) Single AgCl@CMN observed using TEM. The scale bar of the inset is 50 nm. (f) Size distributions of the AgCl@CMNs. (Inset) TEM image of AgCl@CMNs observed in a large area. The scale bar of the inset is 250 nm. (g) High-angle annular dark-field scanning TEM image and elemental maps of CMN after AgCl removal.

confirmed by the binding energy of Ag $3d^{5/2}$ at 367.1 eV.[24] The subsequent photochemical reduction of $AuCl_4^-$ on the AgCl NC templates resulted in the formation of uniform three-dimensional (3D) AgCl@CMNs as observed using both SEM and TEM, demonstrating the selective and preferential reduction of $AuCl_4^-$ on the AgCl NCs via photochemical control (Figure 1d,e). The formation of a significant number of smaller NPs (∼10 nm in diameter) as byproducts along with the AgCl@CMNs on the AgCl NCs was observed in the TEM image (Figure 1e). Although the irregularly shaped byproduct NPs appeared to be connected in the high-resolution TEM image (Figure 1f, inset), their individual particulate morphology and uniform size distribution were identified with the DLS analysis (Figure 1f). These byproduct NPs were further analyzed using the energy-dispersive X-ray spectroscopy and elemental distributions and determined to contain not only Au (62 atom %) but also Ag (38 atom %) with a negligible portion of Cl (<1 atom %), indicating that their formation involves the reduction of the AgCl debris and $HAuCl_4$ (Figure S2). For further clarification *of* the origin of byproduct NPs under similar experimental conditions, we isolated the AgCl debris solution by centrifugation and photochemically reduced them, finally obtaining similar structures and compositions to the Au/Ag alloy byproduct NPs (Figure S3).

The formation of undesired byproducts is a significant obstacle to replication in terms of purity. Therefore, a halogen-free Au precursor $Au(NH_3)_4(NO_3)_3$ was employed as an alternative for the synthesis of CMNs. Due to its moderate standard reduction potential (E° = 0.325 V), it is unlikely that $Au(NH_3)_4^{3+}$ oxidizes Ag to Ag^+ on the AgCl surfaces.[25] Moreover, $Au(NH_3)_4(NO_3)_3$ does not provide Cl^-, eliminating the possibility of the AgCl debris precipitation. The AgCl NCs combined with $Au(NH_3)_4^{3+}$ (64 μM) and a maximum equivalent concentration of NH_3 (256 μM) did not exhibit any noticeable morphological changes (Figure 2a,b). The structural stability of the AgCl NCs in the presence of $Au(NH_3)_4^{3+}$ was

https://doi.org/10.1021/acsomega.3c03096
ACS Omega 2023, 8, 25506−25514

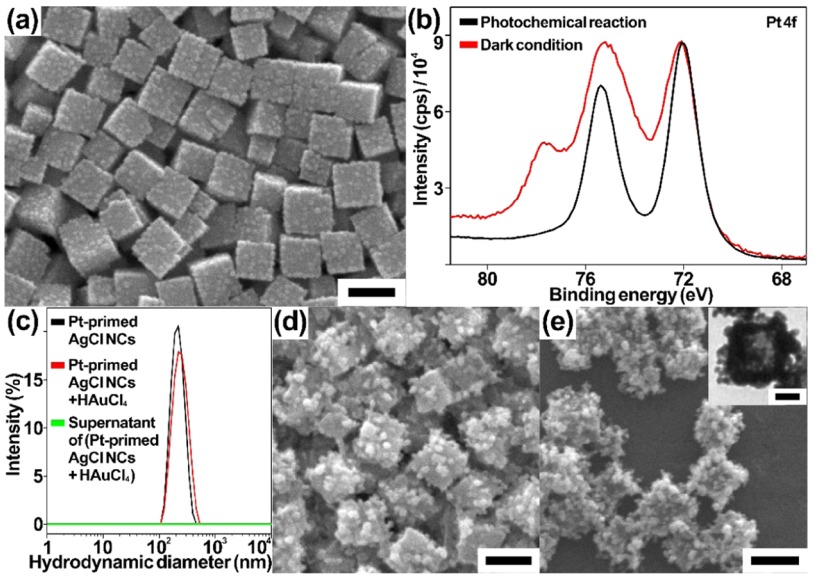

Figure 3. (a) SEM image of Pt-primed AgCl NCs. (b) Pt 4f fine scan spectra of the Pt-primed AgCl NCs synthesized using photochemical reaction (black curve) and reaction with trisodium citrate under dark conditions (red curve). (c) Size distributions of the Pt-primed AgCl NCs before and after the reaction with $HAuCl_4$, and the supernatant solution after the reaction. SEM images of photochemically synthesized (d) AgCl@CMNs and (e) CMNs after the removal of AgCl NCs. (Inset) Magnified TEM image of a single CMN. All of the scale bars are 200 nm except that of the inset which is 50 nm.

demonstrated spectroscopically by obtaining the UV−vis spectra and DLS measurement with negligible changes, which further confirmed the consistent optical properties and size distributions after the mixture formation (Figure 2c,d). As expected, the combination of the AgCl NCs with $Au(NH_3)_4^{3+}$ did not produce any AgCl debris, proving that the mechanistic study of the AgCl debris formation with $AuCl_4^-$ was valid. The photochemical reduction of $Au(NH_3)_4^{3+}$ resulted in the formation of structurally controlled CMNs (edge length = ∼200 nm) with high uniformity (Figure 2e). The DLS measurement as well as the TEM observation of the CMNs did not indicate the presence of the byproduct particles, proofing the validity of a new synthetic route with the least possibility of byproduct formation by using $Au(NH_3)_4^{3+}$ (Figure 2f and inset). The obtained elemental distribution of the CMNs confirmed their bimetallic nature (Au/Ag) with porosity (Figures 2g and S4). In addition to the photochemical reduction of $Au(NH_3)_4^{3+}$, the presence of Ag as a component in the CMN indicates that AgCl templates were partially reduced under synthetic conditions.[3,26] The influence of the selection of the Au precursor on the CMNs after the removal of the AgCl NC templates was investigated (Figure S5). From monitoring the synthesis of the CMNs, uneven growth and consequent bumpy surfaces of the mesh structures on the AgCl NCs were observed with $AuCl_4^-$ that caused poor connectivity and consequent collapse without the support of the AgCl NCs. However, for $Au(NH_3)_4^{3+}$, the mesh grew evenly all over the surface of the AgCl NCs, producing free-standing CMNs after the removal of the AgCl NCs.

Even though the halogen-free $Au(NH_3)_4^{3+}$ as a precursor is attractive due to the purity and free-standing structure of its product CMNs, it is useful to develop an alternative synthetic route for producing free-standing CMNs using conventional $AuCl_4^-$ precursor. The best approach is to prevent the formation of Ag^0 or to completely eliminate it before using $AuCl_4^-$, neither of which is practically possible. So, we hypothesized that coating the AgCl NCs with a layer of another metal would block the $AuCl_4^-$-induced oxidation of Ag^0 on the AgCl NC surfaces. Pt was chosen as a suitable coating material because reduced Pt^0 is expected to be stable in the presence of $AuCl_4^-$ ($E°$ of Pt^{2+} = 1.18 V and $E°$ of $AuCl_4^-$ = 1.002 V). $PtCl_4^{2-}$ is the precursor of our choice as it is not expected to oxidize Ag^0 on the AgCl NCs due to its insufficient reduction potential ($E°$ of $PtCl_4^{2-}$ = 0.755 and $E°$ of Ag^+ = 0.800 V). Unlike $AuCl_4^-$, even if any Cl^- is released from $PtCl_4^{2-}$, there will be no AgCl debris because Ag^0 will not be oxidized. To validate this hypothesis, $PtCl_4^{2-}$ was combined with the AgCl NCs, and it was observed that no debris was produced, indicating that $PtCl_4^{2-}$ did not react with Ag^0 on the AgCl NCs as expected (Figure S6). For the protection of the AgCl NCs, $PtCl_4^{2-}$ underwent further photochemical reduction on the AgCl NCs to wrap them (Pt-primed AgCl NCs). While the AgCl NCs maintained their shape and size, several bumps were observed on the AgCl surfaces after the reduction (Figure 3a). The photochemical reduction of Pt was investigated by analyzing the chemical states of Pt using XPS (Figure 3b). The XPS spectrum of Pt 4f of the photochemically reduced Pt shows the metallic nature of Pt (Pt $4f^{5/2}$ at 75.4 and Pt $4f^{7/2}$ at 72.1 eV), confirming the complete reduction of the $PtCl_4^{2-}$.[27] Removing the AgCl NCs from the Pt-primed AgCl NCs leads to the collapse of the structures composed of thin layers, implying that the Pt^0 coverage on the AgCl NCs was not sufficient enough for mechanical support (Figure S7). The influence of light irradiation on photochemical reduction was evaluated by conducting the reduction reaction under dark conditions. The surface composition of Pt dramatically decreased from 24 to 6 atom %, indicating the reduction was induced by light irradiation. Moreover, the XPS spectrum of the Pt 4f subshell of the Pt-primed AgCl NCs synthesized under dark conditions exhibited an additional higher binding energy at 77.7 eV, implying the presence of Pt cations that are not completely reduced due to the lack of light. The Pt-primed AgCl NCs were combined with $AuCl_4^-$ and examined by DLS, where both Pt-primed AgCl NCs and their

https://doi.org/10.1021/acsomega.3c03096
ACS Omega 2023, 8, 25506−25514

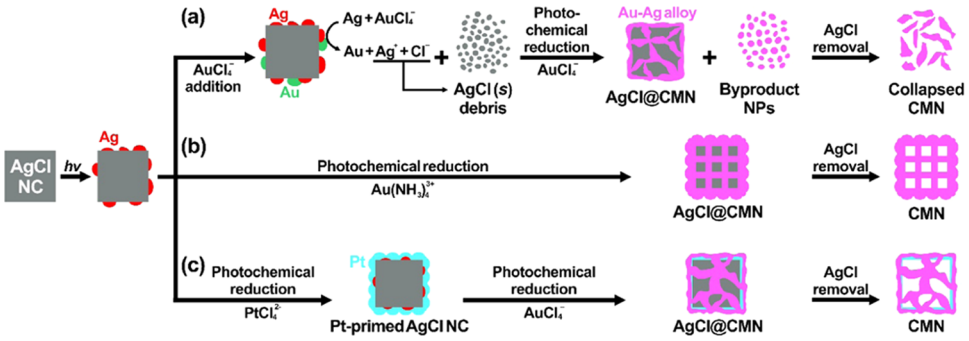

Figure 4. Schematic illustrations of various synthetic routes for CMNs. Synthetic route of CMNs using (a) conventional $AuCl_4^-$ and (b) ligand-exchanged $Au(NH_3)_4^{3+}$ as Au precursors. (c) Alternative synthetic route for replication using Pt-priming and $AuCl_4^-$.

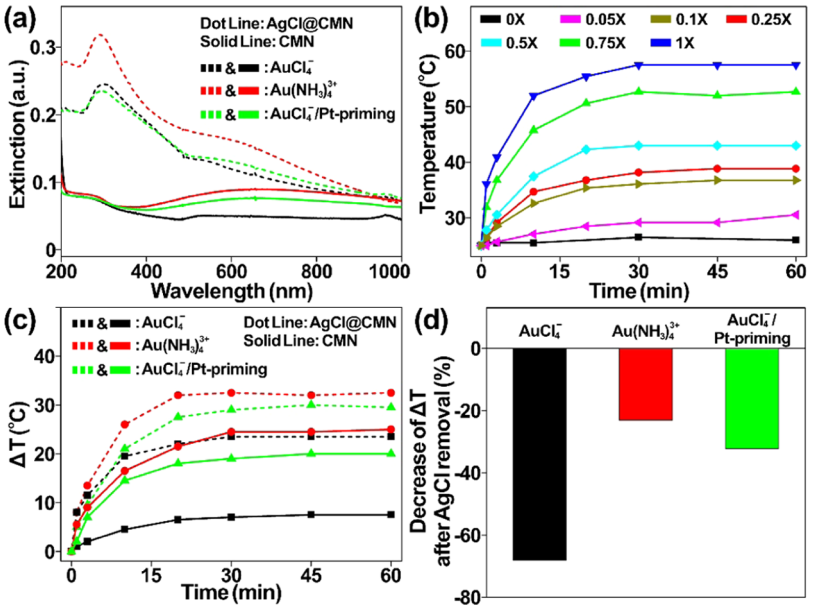

Figure 5. (a) UV−vis absorption spectra of the CMNs before (dot line) and after (solid line) the removal of AgCl NCs. (b) Concentration-dependent temperature changes induced by the $Au(NH_3)_4^{3+}$-based AgCl@CMNs under 808 nm laser irradiation. (c) Temperature increases from 25 °C induced by the three types of the CMNs before (dot line) and after (solid line) the removal of the AgCl NCs. (d) Relative decreases of ΔT_{30}s induced by the CMNs after the removal of the AgCl NCs.

mixture with $AuCl_4^-$ showed uniform size distribution (Figure 3c). The supernatant of the mixture did not contain any AgCl debris, successfully proving the protective function of Pt for Ag^0 on the AgCl NCs from $AuCl_4^-$. The subsequent reduction of $AuCl_4^-$ on the Pt-primed AgCl NCs resulted in the CMNs around the AgCl NCs (Figure 3d). Despite their uneven surface morphologies, the AgCl@CMNs maintained their cubic structures even after the removal of the AgCl NC templates (Figure 3e). This result proposes that the surface protection of the AgCl NCs by wrapping inert metallic layers is a solution for synthesizing the CMNs without any impurity issues caused by conventional $AuCl_4^-$.

The investigated synthetic routes for the CMNs are illustrated in Figure 4. In Figure 4a, it is noteworthy that the metallic silver (Ag^0) on the photosensitive AgCl NCs causes the production of undesired impurities when used with $AuCl_4^-$ precursor because it is highly oxidative and releases Cl^- ions. Unless the AgCl NCs are synthesized in a dark room without any light source, which is impossible, the formation of the solid AgCl debris and its subsequent conversion to the Au/Ag alloy byproduct NPs is inevitable. Although there are several reports on AgCl nanostructures with $AuCl_4^-$, to the best of our knowledge, this is the first report associated with the undesired formation of AgCl debris from a mixture of the AgCl NCs and $AuCl_4^-$, as the tiny size and small quantity of debris make its identification highly challenging.[1,6,10] The CMNs collapse after the removal of the template possibly due to a deficiency of Au that was partially consumed during the formation of byproduct NPs. In Figure 4b, we propose a fundamental solution to this issue using a new ligand-exchanged Au precursor, $Au(NH_3)_4^{3+}$, which is less oxidative and contains no halogen element. As expected, no side reactions were observed, resulting in the formation of free-standing CMNs. In Figure 4c, an alternative route is developed to protect the AgCl NCs, including Ag^0 on the surface, which allows the use of conventional $AuCl_4^-$ for the synthesis of free-standing CMNs. $PtCl_4^{2-}$ is chosen as a protector because of its suitable reduction potential that is not high enough for oxidizing Ag^0 but still sufficient for photochemical reduction. As Ag^0 is not oxidized, the AgCl debris was not formed despite the Cl^- ions released from $PtCl_4^{2-}$. Eventually, this last method demonstrates the successful formation of free-standing CMNs using the conventional Au precursor by taking advantage of the Pt-priming. The two successful routes for the formation of free-

https://doi.org/10.1021/acsomega.3c03096
ACS Omega 2023, 8, 25506−25514

standing CMNs (Figure 4b,c) are also applicable to the photochemical replication of the AgCl nanospheres (AgCl NSs) for synthesizing spherical mesh nanostructures (SMNs) (Figure S8).

Lastly, the structural stability of the synthesized CMNs was investigated comparatively with three chemical approaches ($AuCl_4^-$, $Au(NH_3)_4^{3+}$, and $AuCl_4^-$/Pt-priming). As typical electron microscopic methods provide only local observation of a few CMNs, an additional evaluation is required for the global examination of the entire CMNs. Although X-ray diffraction and light-scattering-based methods evaluate the overall properties of the products, they only verify the atomic crystallinity and size distribution and do not provide a sufficient understanding of the structural properties on the tens of nanometer scale. Based on this reasoning, we decided to take advantage of spectroscopic approaches that directly correlate with localized surface plasmon resonance (LSPR) and the photothermal properties of the hollow Au/Ag nanomaterials such as CMNs, both of which strongly depend on the structures.[28,29] The analysis of the temperature increase induced by the CMNs would be a precise and convenient measure for evaluating the structural stability of CMNs before and after the removal of the AgCl NC templates. We first observed the UV−vis spectra of the three types of AgCl@CMNs to determine the wavelength of the light irradiation (Figure 5a). Since the core AgCl NCs exhibited strong absorption bands around 300 nm (Figure 2c), the optical properties of the AgCl@CMNs were determined mainly based on the AgCl NC templates before their removal. Due to the presence of the CMNs, broad plasmonic absorption bands were also observed in the visible and near-infrared (NIR) regions. These LSPR-based optical properties were more pronounced for the $Au(NH_3)_4^{3+}$-based and $AuCl_4^-$/Pt-priming-based CMNs after the removal of the AgCl templates. Unlike the other two, the $AuCl_4^-$-based CMNs exhibited almost a flat spectrum, probably due to structural collapse after the removal of AgCl NCs as shown in Figure S5. The photothermal properties of the three AgCl@CMNs were investigated by observing temperature changes under 808 nm laser irradiation (1 W/cm^2) (Figure S9). The three types of CMNs exhibited maximum temperatures in 30 min, among which the $Au(NH_3)_4^{3+}$-based AgCl@CMNs were observed to be the most photothermally efficient. Subsequently, we confirmed the concentration-dependent photothermal properties of the $Au(NH_3)_4^{3+}$-based AgCl@CMNs (Figure 5b). Lastly, to analyze the overall structural stability of the CMNs, we compared the photothermal properties of the CMNs before and after the removal of the AgCl NCs. As the temperature stopped increasing at 30 min with all of the CMNs, the temperature increase from 25 °C at 30 min (ΔT_{30}) was used as a measure to evaluate the type- and time-dependent structural stability of the CMNs (Figure 5c). Regardless of the type of the AgCl@CMNs, the ΔT_{30}'s dropped after the removal of the AgCl NCs (dot line → solid line), indicating that the partial collapse of the CMN structures occurred in common. Specifically, the photothermal properties of the $Au(NH_3)_4^{3+}$-based and $AuCl_4^-$/Pt-priming-based CMNs were still pronounced even after the AgCl removal, exhibiting ΔT_{30}s of 25 and 20 °C, respectively. In contrast, the $AuCl_4^-$-based CMNs only showed a ΔT_{30} of 7.5 °C. For the relative comparison of these ΔT_{30}'s, the percentage decrease of the ΔT_{30} was calculated and is shown in Figure 5d. Since the $AuCl_4^-$-based CMNs rarely maintained the structures after the AgCl template removal, the ΔT_{30} largely decreased by 68%. However, the other two stable CMNs resulted in only a 23 and 32% decrease of the ΔT_{30}, respectively. Based on the photothermal activities, the $Au(NH_3)_4^{3+}$-based CMNs appeared to exhibit the highest structural stability, which was additionally proved by their plasmon-enhanced photocatalytic properties for the degradation of harmful Cr^{6+} (Figure S10). This investigation demonstrates that the photothermal properties can be a suitable analytical tool that supports microscopic methods such as TEM, for evaluating the overall structural properties of hollow Au/Ag nanostructures, particularly with an emphasis on stability.

CONCLUSIONS

AgCl has been used as a nanostructured template for the convenient synthesis of complicated multimetallic nanomaterials in aqueous media. However, it is still unclear how its replication is impacted by its complex chemistry, such as its photosensitivity, redox reactions, and water solubility. This study demonstrated the precursor-dependent synthesis of the bimetallic CMNs using three distinctive but related methods, verifying that the type of precursor ligands significantly affects the structural stability and purity of the resultant CMNs. By unveiling that $AuCl_4^-$ induces the formation of undesirable byproducts owing to its high oxidizing power and presence of Cl^- ion, we were able to synthesize pure and structurally stable CMNs using a halogen-free Au precursor. Moreover, we proposed an alternative method by taking advantage of Pt-priming, which is based on the electrochemical potential of Pt as a key to the reliable use of conventional $AuCl_4^-$ for the synthesis of the CMNs. Lastly, photothermal properties were suggested as a new measure for evaluating the overall structural stability of the replicated CMNs. Considering other water-insoluble silver halides as potential nano-templates, our new discovery of the purity and stability issues of the AgCl replication is a solid and general reference for the synthesis of functional noble metal nanomaterials for photocatalysis, biological probes, and photothermal therapy.[30−32]

ASSOCIATED CONTENT

Supporting Information

The Supporting Information is available free of charge at https://pubs.acs.org/doi/10.1021/acsomega.3c03096.

Additional SEM and TEM images, elemental maps, DLS spectra, and photothermal and photocatalytic analysis (PDF)

AUTHOR INFORMATION

Corresponding Author

Jae-Seung Lee − *Department of Materials Science and Engineering, Korea University, Seoul 02841, Republic of Korea*; orcid.org/0000-0002-4077-2043; Email: JSLEE79@korea.ac.kr

Authors

Han-Jung Ryu − *Department of Materials Science and Engineering, Korea University, Seoul 02841, Republic of Korea*

Kyung Tae Kim − *Department of Materials Science and Engineering, Korea University, Seoul 02841, Republic of Korea*

https://doi.org/10.1021/acsomega.3c03096
ACS Omega 2023, 8, 25506−25514

Won Kyu Lee − *Department of Materials Science and Engineering, Korea University, Seoul 02841, Republic of Korea*

Complete contact information is available at: https://pubs.acs.org/10.1021/acsomega.3c03096

Notes

The authors declare no competing financial interest.

■ ACKNOWLEDGMENTS

This work was supported by BK21 FOUR Program through the National Research Foundation of Korea (NRF) funded by the Ministry of Education (4199990514635) and by the NRF grant funded by the Ministry of Science and ICT (RS-2023-00207833 and NRF-2021R1A2C1012917). Elemental maps, ICP-MS data, and XPS spectra were obtained from the Seoul, Daegu, and Busan Centers of the Korea Basic Science Institute (KBSI, Republic of Korea), respectively.

■ REFERENCES

(1) Pedireddy, S.; Lee, H. K.; Tjiu, W. W.; Phang, I. Y.; Tan, H. R.; Chua, S. Q.; Troadec, C.; Ling, X. Y. One-step Synthesis of Zero-dimensional Hollow Nanoporous Gold Nanoparticles with Enhanced Methanol Electrooxidation Performance. *Nat. Commun.* **2014**, *5*, No. 4947.

(2) Ryu, H. J.; Shin, H.; Oh, S.; Joo, J. H.; Choi, Y.; Lee, J. S. Wrapping AgCl Nanostructures with Trimetallic Nanomeshes for Plasmon-Enhanced Catalysis and in Situ SERS Monitoring of Chemical Reactions. *ACS Appl. Mater. Interfaces* **2020**, *12*, 2842−2853.

(3) Joo, J. H.; Kim, B. H.; Lee, J. S. Synthesis of Gold Nanoparticle-Embedded Silver Cubic Mesh Nanostructures Using AgCl Nanocubes for Plasmonic Photocatalysis. *Small* **2017**, *13*, No. 1701751.

(4) Liu, S.; Chai, J.; Sun, S. A.; Zhang, L.; Yang, J. Y.; Fu, X.; Hai, J.; Jing, Y. H.; Wang, B. D. Site-Selective Photosynthesis of Ag-AgCl@Au Nanomushrooms for NIR-II Light-Driven O_2- and $O_2^{\bullet-}$-Evolving Synergistic Photothermal Therapy against Deep Hypoxic Tumors. *ACS Appl. Mater. Interfaces* **2021**, *13*, 46451−46463.

(5) Ye, Z. W.; Li, C. C.; Celentano, M.; Lindley, M.; O'Reilly, T.; Greer, A. J.; Huang, Y. M.; Hardacre, C.; Haigh, S. J.; Xu, Y. K.; Bell, S. E. J. Surfactant-free Synthesis of Spiky Hollow Ag-Au Nanostars with Chemically Exposed Surfaces for Enhanced Catalysis and Single-Particle SERS. *JACS Au* **2022**, *2*, 178−187.

(6) Li, J. R.; Zhang, G. N.; Wang, J.; Maksymov, I. S.; Greentree, A. D.; Hu, J. M.; Shen, A. G.; Wang, Y. L.; Trau, M. Facile One-Pot Synthesis of Nanodot-Decorated Gold-Silver Alloy Nanoboxes for Single-Particle Surface-Enhanced Raman Scattering Activity. *ACS Appl. Mater. Interfaces* **2018**, *10*, 32526−32535.

(7) Bian, K. X.; Zhang, X. W.; Liu, K.; Yin, T.; Liu, H.; Niu, K.; Cao, W. W.; Gao, D. W. Peptide-Directed Hierarchical Mineralized Silver Nanocages for Anti-Tumor Photothermal Therapy. *ACS Sustainable Chem. Eng.* **2018**, *6*, 7574−7588.

(8) Tan, Y. N.; Yang, J.; Lee, J. Y.; Wang, D. I. C. Mechanistic Study on the Bis(p-sulfonatophenyl)phenylphosphine Synthesis of Monometallic Pt Hollow Nanoboxes Using Ag*-Pt Core-shell Nanocubes as Sacrificial Templates. *J. Phys. Chem. C* **2007**, *111*, 14084−14090.

(9) Lu, Y. X.; Qin, Y. Z.; Yu, D. D.; Zhou, J. G. Stepwise Evolution of AgCl Microcrystals from Octahedron into Hexapod with Mace Pods and their Visible Light Photocatalytic Activity. *Crystals* **2019**, *9*, 401.

(10) Ryu, H. J.; Kim, H. L.; Joo, J. H.; Lee, J. S. Structurally and Compositionally Tunable Absorption Properties of AgCl@AgAu Nanocatalysts for Plasmonic Photocatalytic Degradation of Environmental Pollutants. *Catalysts* **2020**, *10*, 405.

(11) Singh, A.; Hou, W. C.; Lin, T. F.; Zepp, R. G. Roles of Silver-Chloride Complexations in Sunlight-Driven Formation of Silver Nanoparticles. *Environ. Sci. Technol.* **2019**, *53*, 11162−11169.

(12) Zhou, S.; Li, J. H.; Gilroy, K. D.; Tao, J.; Zhu, C. L.; Yang, X.; Sun, X. J.; Xia, Y. N. Facile Synthesis of Silver Nanocubes with Sharp Corners and Edges in an Aqueous Solution. *ACS Nano* **2016**, *10*, 9861−9870.

(13) Maudos, I.; Chimenos, J. M.; Segarra, M.; Espiell, F. Kinetic Study of Silver Chloride Dissolution in Complexating Media. *Hydrometallurgy* **1996**, *40*, 153−167.

(14) Yang, T. H.; Peng, H. C.; Zhou, S.; Lee, C. T.; Bao, S. X.; Lee, Y. H.; Wu, J. M.; Xia, Y. N. Toward a Quantitative Understanding of the Reduction Pathways of a Salt Precursor in the Synthesis of Metal Nanocrystals. *Nano Lett.* **2017**, *17*, 334−340.

(15) Yang, T. H.; Gilroy, K. D.; Xia, Y. N. Reduction Rate as a Quantitative Knob for Achieving Deterministic Synthesis of Colloidal Metal Nanocrystals. *Chem. Sci.* **2017**, *8*, 6730−6749.

(16) Turkevich, J.; Stevenson, P. C.; Hillier, J. A Study of the Nucleation and Growth Processes in the Synthesis of Colloidal Gold. *J. Discuss. Faraday Soc.* **1951**, *11*, 55−75.

(17) Wang, S.; Qian, K.; Bi, X. Z.; Huang, W. X. Influence of Speciation of Aqueous $HAuCl_4$ on the Synthesis, Structure, and Property of Au Colloids. *J. Phys. Chem. C* **2009**, *113*, 6505−6510.

(18) Ryu, H. J.; Lee, W. K.; Choi, J. Y.; Lee, J. S. Silver Halide-induced Catalyst Poisoning of Ag-M Bimetallic Nanoparticles (biNPs) and Their Chemical Regeneration. *J Alloy Compd.* **2022**, *899*, No. 163260.

(19) Lee, W. K.; Kwon, K.; Choi, Y.; Lee, J. S. Dynamic Metallization of Spherical DNA Via Conformational Transition into Gold Nanostructures with Controlled Sizes and Shapes. *J. Colloid Interface Sci.* **2021**, *594*, 160−172.

(20) Skibsted, L. H.; Bjerrum, J. Studies on Gold Complexes. 1. Robustness, Stability and Acid Dissociation of Tetramminegold(III) Ion. *Acta Chem. Scand.* **1974**, *A 28*, 740−746.

(21) Shim, J. H.; Yang, J.; Kim, S. J.; Lee, C.; Lee, Y. One Dimensional Ag/Au/AgCl Nanocomposites Stemmed from Ag Nanowires for Electrocatalysis of Oxygen Reduction. *J. Mater. Chem.* **2012**, *22*, 15285−15290.

(22) Yang, Y.; Zhao, Y.; Yan, Y. K.; Wang, Y. L.; Guo, C. Y.; Zhang, J. S. Preparation of AgCl Nanocubes and Their Application as Efficient Photoinitiators in the Polymerization of N-Isopropylacrylamide. *J. Phys. Chem. B* **2015**, *119*, 14807−14813.

(23) Wang, G.; Nishio, T.; Sato, M.; Ishikawa, A.; Nambara, K.; Nagakawa, K.; Matsuo, Y.; Niikura, K.; Ijiro, K. Inspiration from Chemical Photography: Accelerated Photoconversion of AgCl to Functional Silver Nanoparticles Mediated by DNA. *Chem. Commun.* **2011**, *47*, 9426−9428.

(24) Al-Sarraj, A.; Saoud, K. M.; Elmel, A.; Mansour, S.; Haik, Y. Optoelectronic Properties of Highly Porous Silver Oxide Thin Film. *SN Appl. Sci.* **2021**, *3*, 15.

(25) Skibsted, L. H.; Bjerrum, J. Studies on Gold Complexes. 2. Equilibrium between Gold(I) and Gold(III) in Ammonia System and Standard Potentials of Couples Involving Gold, Diamminegold(I), and Tetramminegold(III). *Acta Chem. Scand.* **1974**, *A 28*, 764−770.

(26) Chew, W. S.; Pedireddy, S.; Lee, Y. H.; Tjiu, W. W.; Liu, Y. J.; Yang, Z.; Ling, X. Y. Nanoporous Gold Nanoframes with Minimalistic Architectures: Lower Porosity Generates Stronger Surface-Enhanced Raman Scattering Capabilities. *Chem. Mater.* **2015**, *27*, 7827−7834.

(27) Zhang, B.; Zhu, H.; Zou, M. L.; Liu, X. R.; Yang, H.; Zhang, M.; Wu, W. W.; Yao, J. M.; Du, M. L. Design and Fabrication of Size-Controlled Pt-Au Bimetallic alloy Nanostructure in Carbon Nanofibers: A Bifunctional Material for Biosensors and the Hydrogen Evolution Reaction. *J. Mater. Sci.* **2017**, *52*, 8207−8218.

(28) Lv, Z. Q.; He, S. J.; Wang, Y. F.; Zhu, X. Y. Noble Metal Nanomaterials for NIR-Triggered Photothermal Therapy in Cancer. *Adv. Healthcare Mater.* **2021**, *10*, No. 2001806.

(29) Genç, A.; Patarroyo, J.; Sancho-Parramon, J.; Bastus, N. G.; Puntes, V.; Arbiol, J. Hollow Metal Nanostructures for Enhanced

Plasmonics: Synthesis, Local Plasmonic Properties and Applications. *Nanophotonics* **2017**, *6*, 193−213.
(30) Reddy, N. L.; Rao, V. N.; Vijayakumar, M.; Santhosh, R.; Anandan, S.; Karthik, M.; Shankar, M. V.; Reddy, K. R.; Shetti, N. P.; Nadagouda, M. N.; Aminabhavi, T. M. A Review on Frontiers in Plasmonic Nano-photocatalysts for Hydrogen Production. *Int. J. Hydrogen Energy* **2019**, *44*, 10453−10472.
(31) Azharuddin, M.; Zhu, G. H.; Das, D.; Ozgur, E.; Uzun, L.; Turner, A. P. F.; Patra, H. K. A Repertoire of Biomedical Applications of Noble Metal Nanoparticles. *Chem. Commun.* **2019**, *55*, 6964−6996.
(32) Xu, J. W.; Yao, K.; Xu, Z. K. Nanomaterials with a Photothermal Effect for Antibacterial Activities: An Overview. *Nanoscale* **2019**, *11*, 8680−8691.

https://doi.org/10.1021/acsomega.3c03096
ACS Omega 2023, 8, 25506−25514